

Density Functional Theory for Hard Polyhedra

Matthieu Marechal and Hartmut Löwen

Institut für Theoretische Physik II, Heinrich-Heine-Universität Düsseldorf, Universitätsstraße 1, 40225 Düsseldorf, Germany
(Received 25 October 2012; published 25 March 2013)

Using the framework of geometry-based fundamental-measure theory, we develop a classical density functional for hard polyhedra and their mixtures and apply it to inhomogeneous fluids of Platonic solids near a hard wall. As revealed by Monte Carlo simulations, the faceted shape of the polyhedra leads to complex layering and orientational ordering near the wall, which is excellently reproduced by our theory. These effects can be verified in real-space experiments on polyhedral colloids.

DOI: [10.1103/PhysRevLett.110.137801](https://doi.org/10.1103/PhysRevLett.110.137801)

PACS numbers: 61.20.Gy, 05.20.Jj, 61.30.Hn, 82.70.Dd

Recent advances in the controlled preparation of anisotropic nanoparticles and colloids have boosted our understanding of the collective properties of orientable hard polyhedra. In fact, it is by now possible to prepare micro-to nanometric particles with a polyhedral shape [1–5]. These particles self-assemble into structures much more complex than those formed by spheres and are therefore ideal candidates for photonic crystals [6] or electrical networks [7]. At a very high concentration, the structure should resemble the best-packed configurations of polyhedra, the determination of which is a geometric problem dating back to Plato [8] and is still under debate today in connection with Ulam’s conjecture [9]. The latter states that spheres have the lowest maximal packing fraction of all convex shapes and was confirmed for a large number of polyhedra [9–11] but not yet proved in general. At densities below close packing, new structures were discovered by computer simulation which are vastly different from the close-packed ones [12–15]. A spectacular example is a decagonal quasicrystal formed by hard tetrahedra [12,16] and triangular bipyramids [13].

However, a general microscopic theory for the structure and phase behavior of hard polyhedra is missing. Previous theories for hard tetrahedra [17,18], motivated by the shapes of molecules such as CF_4 and CH_4 [19], did not explicitly take the orientations into account. Here, we will use classical density functional theory (DFT) with explicit orientational degrees of freedom. By its design, DFT provides a powerful, microscopic tool to investigate inhomogeneous fluids [20–22]. A geometry-based fundamental-measure theory was proposed for hard spheres by Rosenfeld [23,24], which was later generalized to hard particles with an arbitrary smooth shape by Hansen-Goos and Mecke [25,26]. The fundamental-measure theory has been proven to be very successful for inhomogeneous hard sphere fluids [27], including the crystalline state [28] and the fluid-solid interface, as well as for inhomogeneous fluids of hard spherocylinders [25]. In particular, studies of the fluid-solid interface [29] and the interface between a fluid and a hard wall [27] for hard spheres illustrate clearly the usefulness of DFT, which directly yields the free energy and,

thus, the interfacial tension, while the complementary simulation approaches are much more computationally demanding [29–31].

In this Letter, we use the framework of geometry-based fundamental-measure theory [25,26] and generalize it to sharp edged hard polyhedra and their mixtures. We consider Platonic solids, in particular; see Fig. 1. The density functional theory is applied to the standard test case, namely, to inhomogeneous fluids near a hard wall, and we perform Monte Carlo computer simulations for comparison. The faceted shape of the polyhedra leads to complex layering and orientational ordering near the wall, which are excellently reproduced by our theory. We find layering effects that are not compatible with the behavior expected from close-packed ordering for a mixture of tetrahedra and octahedra. In principle, our theory can be exploited for structural ordering and bulk phase transitions for particles with an arbitrary polyhedral shape. It will also be paramount in understanding the heterogeneous nucleation of crystals or mesophases at a wall. As was already demonstrated for spherical particles [32,33], the predicted layering effects near walls can be verified in confocal microscopy experiments on sterically stabilized anisotropic colloids.

Density functional theory is specifically designed to handle inhomogeneous mixtures of anisotropic particles described by a density profile $\rho_s(\mathbf{r}, \boldsymbol{\varpi})$, which expresses the local density at the position \mathbf{r} of particles of a certain species s with a specific orientation $\boldsymbol{\varpi}$, which denotes the three Euler angles. The grand-canonical free energy—the thermodynamic potential of the ensemble where the chemical potential μ , the volume V , and the temperature T are held fixed—can be written as a sum over three parts

$$\Omega = \mathcal{F}_{\text{id}} + \mathcal{F}_{\text{exc}} + \sum_s \int d\boldsymbol{\varpi} \int d\mathbf{r} \rho_s(\mathbf{r}, \boldsymbol{\varpi}) [V_s^{\text{ext}}(\mathbf{r}, \boldsymbol{\varpi}) - \mu],$$

where $V_s^{\text{ext}}(\mathbf{r}, \boldsymbol{\varpi})$ is the external potential. The first term in the grand potential Ω is the ideal gas free energy [20] $\mathcal{F}_{\text{id}} = k_B T \sum_s \iint \rho_s(\mathbf{r}, \boldsymbol{\varpi}) \log[\rho_s(\mathbf{r}, \boldsymbol{\varpi}) \mathcal{V}] - \rho_s(\mathbf{r}, \boldsymbol{\varpi}) d\boldsymbol{\varpi} d\mathbf{r}$, where k_B is Boltzmann’s constant and \mathcal{V} is the irrelevant thermal volume. The excess free energy from fundamental-measure theory [23–26,34] reads

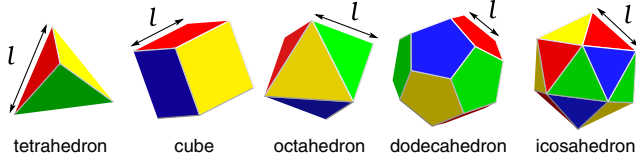


FIG. 1 (color online). The polyhedra considered in this work are tetrahedra, cubes (hexahedra), octahedra, dodecahedra, and icosahedra with (equal) edge lengths l as indicated. The different colors are simply to allow facile distinction of the faces.

$\mathcal{F}_{\text{exc}} = k_B T \int d\mathbf{r} \Phi(\{n_{\alpha,\tau}(\mathbf{r})\})$ in terms of scalar ($\tau = 0$), vector ($\tau = 1$), and rank-two tensor ($\tau = 2$) weighted densities denoted by $n_{\alpha,\tau}(\mathbf{r})$, where $\alpha = 0, \dots, 3$.

The function $\Phi(\{n_{\alpha,\tau}\})$ of the set of weighed densities $\{n_{\alpha,\tau}\}$ reads

$$-n_0 \log(1 - n_3) + \frac{n_1 n_2 - \vec{n}_1 \cdot \vec{n}_2 - \text{Tr}[\vec{n}_1 \vec{n}_2]}{1 - n_3} + \frac{3}{16\pi} \frac{\vec{n}_2 \cdot \vec{n}_2 \vec{n}_2 - n_2 \vec{n}_2 \cdot \vec{n}_2 + n_2 \text{Tr}[\vec{n}_2^2] - \text{Tr}[\vec{n}_2^3]}{(1 - n_3)^2},$$

where we use the notation $n_\alpha \equiv n_{\alpha,0}$, $\vec{n}_\alpha \equiv n_{\alpha,1}$, and $\vec{n}_\alpha \equiv n_{\alpha,2}$ to emphasize the scalar, vector, and tensor nature of the corresponding weighted densities and Tr denotes the trace of a matrix.

For brevity, we will call the polyhedron of species s with orientation ϖ polyhedron ν . The weighted densities contain convolutions of the density profile with weight functions $w_\nu^{(\alpha,\tau)}(\mathbf{r}')$, which are only known for smooth particles [26]. To extend the weight functions to polyhedra, we first consider rounded polyhedra, where the edges are replaced by cylinder sections with radius R and the vertices by any surface that connects the rounded edges and faces smoothly. For convenience, we calculate the Fourier transformed weight functions $\hat{w}_\nu^{(\alpha,\tau)}(\mathbf{k})$ for such rounded polyhedra and we perform the limit $R \rightarrow 0$. A more detailed derivation of the weight functions is given in the Supplemental Material [35]. The resulting Fourier transformed weight functions are

$$\hat{w}_\nu^{(\alpha,\tau)}(\mathbf{k}) = \sum_{j=1}^{N_{\alpha,\nu}} \xi_\nu^{(\alpha,\tau)} \hat{\delta}_{\alpha,\nu,j}(\mathbf{k})$$

by dividing polyhedron ν into $N_{3,\nu}$ irregular tetrahedra and its surface into $N_{2,\nu}$ triangles, while $N_{1,\nu}$ is the number of edges for polyhedron ν and $N_{0,\nu}$ is the number of vertices. Also, we define the delta-like function $\delta_{\alpha,\nu,j}(\mathbf{r})$ by $\int d\mathbf{r} f(\mathbf{r}) \delta_{\alpha,\nu,j}(\mathbf{r}) = \int_{S_{\alpha,\nu,j}} d\mathbf{r} f(\mathbf{r})$ for any function $f(\mathbf{r})$, where $S_{\alpha,\nu,j}$ is an α -dimensional simplex: $S_{0,\nu,j}$ denotes vertex j , $S_{1,\nu,j}$ denotes edge j , triangle j is denoted by $S_{2,\nu,j}$, and, finally, we denote the j th irregular tetrahedron by $S_{3,\nu,j}$. The subdivision of the surface and interior of the particle in these simplices $S_{\alpha,\nu,j}$ allows the following closed

form to be derived for the Fourier transform $\hat{\delta}_{\alpha,\nu,j}(\mathbf{k})$ of the delta-like function:

$$\alpha! |S_{\alpha,\nu,j}| \sum_{n=1}^{\alpha+1} \frac{\exp(-i\mathbf{k} \cdot \mathbf{r}_{\alpha,\nu,j,n})}{\prod_{m=1, m \neq n}^{\alpha+1} i\mathbf{k} \cdot (\mathbf{r}_{\alpha,\nu,j,m} - \mathbf{r}_{\alpha,\nu,j,n})},$$

where $|S_{\alpha,\nu,j}|$ is 1 for $\alpha = 0$ and is equal to the length, area, and volume of the j th edge, triangle, and irregular tetrahedron for $\alpha = 1, 2$, and 3, respectively, of polyhedron s . Also, the n th vertex of the j th α simplex of polyhedron ν is denoted by $\mathbf{r}_{\alpha,\nu,j,n}$. The \mathbf{k} -independent $\xi_s^{(\alpha,\tau)}$ consist of scalars ($\tau = 0$), $\xi_\nu^{(0,0)} \equiv [2\pi - \sum_{k=1}^{F_{\nu,j}} \angle(\nu, j, k)]/4\pi$, $\xi^{(1,0)} \equiv \sigma_{\nu,j} \phi_{\nu,j}/8\pi$, $\xi^{(2,0)} \equiv 1$, and $\xi^{(3,0)} \equiv 1$; vectors ($\tau = 1$), $\xi^{(1,1)} \equiv \mathbf{e}_{\nu,j,3} \sin(\phi_{\nu,j}/2)/4\pi$, and $\xi^{(2,1)} \equiv \mathbf{n}_{\nu,j}$; and, finally, rank-two tensors ($\tau = 2$), $\xi^{(1,2)} \equiv \sigma_{\nu,j} [\sin \phi_{\nu,j} (\mathbf{e}_{\nu,j,1} \mathbf{e}_{\nu,j,1}^T - \mathbf{e}_{\nu,j,2} \mathbf{e}_{\nu,j,2}^T) - (\phi_{\nu,j} + \sin \phi_{\nu,j}) (\frac{3}{2} \mathbf{e}_{\nu,j,1} \mathbf{e}_{\nu,j,1}^T - \frac{1}{2} \mathbb{I})]/8\pi$ and $\xi^{(2,2)} \equiv \mathbf{n}_{\nu,j} \mathbf{n}_{\nu,j}^T$, where $\angle(\nu, j, k)$ is the opening angle of face k of the $F_{\nu,j}$ faces joined at vertex j , $\phi_{\nu,j}$ denotes the angle between the two normals $\mathbf{n}_{\nu,j,1}$ and $\mathbf{n}_{\nu,j,2}$ of the faces joined in edge j , $\sigma_{\nu,j}$ is 1 (−1) if the surface near edge j is convex (concave), $\mathbf{e}_{\nu,j,1} = \mathcal{N}[\mathbf{n}_{\nu,j,1} \times \mathbf{n}_{\nu,j,2}]$, $\mathbf{e}_{\nu,j,2} = \mathcal{N}[\mathbf{n}_{\nu,j,1} - \mathbf{n}_{\nu,j,2}]$, and $\mathbf{e}_{\nu,j,3} = \mathcal{N}[\mathbf{n}_{\nu,j,1} + \mathbf{n}_{\nu,j,2}]$ with $\mathcal{N}[\mathbf{v}] = \mathbf{v}/|\mathbf{v}|$, and finally $\mathbf{n}_{\nu,j}$ is the normal of face j .

Using these expressions for the weight functions, we can calculate the Fourier transformed weighted densities

$$\hat{n}_{\alpha,\tau}(\mathbf{k}) = \sum_s \int d\varpi \hat{w}_s^{(\alpha,\tau)}(\mathbf{k}, \varpi) \hat{\rho}_s(\mathbf{k}, \varpi),$$

where $\hat{\rho}_s(\mathbf{k}, \varpi)$ denotes the Fourier transform of the density. Finally, the free energy is minimized with respect to the density profile using the Picard iteration [27].

First, we will consider one-component fluids of the Platonic solids (see Fig. 1) near a hard wall. The hard wall leads to an external potential $V_s^{\text{ext}}(\mathbf{r}, \varpi)$, which is infinite if a particle of species s with orientation ϖ at position \mathbf{r} overlaps with the wall and zero otherwise. We compare our theory to standard Monte Carlo simulations of polyhedra confined between two walls at large enough separation L [35] that the middle of the slit behaves like a bulk fluid. To limit the parameter space, we will fix the average packing fraction $\eta \equiv v_p N/(LA)$ to $\eta = 0.3$, where v_p is the volume of the particle, N is the number of particles, and A is the area of the plates. For this volume fraction, we always find a fluid phase.

In Fig. 2, the results for the dimensionless center-of-mass density profile $\eta(z) \equiv v_p \sum_{i=1}^N \langle \delta(z - z_i) \rangle$ are shown, where z_i is the distance between the center of mass of polyhedron i and the wall (the wall separation L is at least 4 times larger than the z interval shown). First of all, the comparison between the simulation results and the theory is good for tetrahedra and excellent for all other Platonic solids. The structure of the peak near the wall is a result of a competition of two effects: the pressure of the particles in

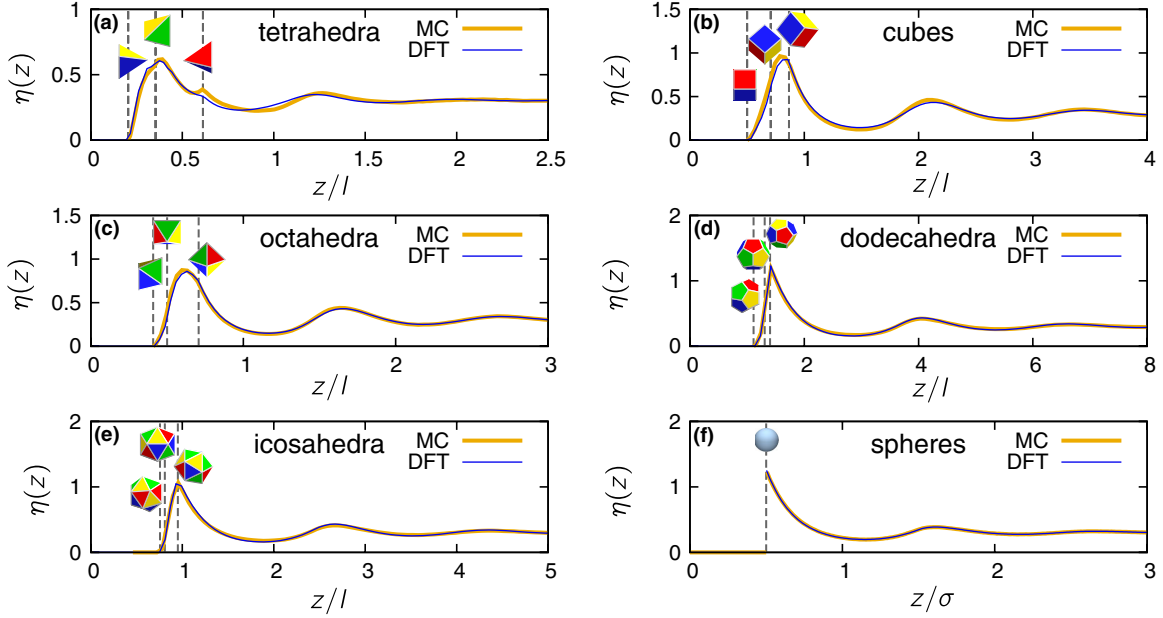


FIG. 2 (color online). Center-of-mass density profiles as a function of the height z divided by the edge length l for one-component systems of (a) tetrahedra, (b) cubes, (c) octahedra, (d) dodecahedra, and (e) icosahedra, which are depicted in Fig. 1. Fundamental-measure DFT (dark or blue lines) is compared to results from Monte Carlo (MC) simulations (light or orange lines). The average volume fraction $\eta \equiv v_p N/AH$ is set to $\eta = 0.3$, where v_p is the volume of the particles. (f) The density profile of spheres for the same packing fraction $\eta = 0.3$ is shown as a function of the height z divided by the diameter σ for comparison. The heights for which a particle can just touch the wall with a vertex, an edge, and a face are indicated by the dashed lines; also shown are polyhedra with the corresponding orientations.

the bulk that pushes the particles in the first layer toward the wall and the rotational entropy loss that the particles near the wall suffer because some of the orientations are excluded due to overlap with the wall. The interplay between these effects causes a complex layering, where for instance tetrahedra show a sharp feature in between the peaks of the first and second layers. Also, whether the first peak is a sharp peak or a broad peak depends critically on the shape of the particle. The maximum wall distance for which a vertex, edge, or face can touch the wall (denoted by z_v , z_e , and z_f , respectively) is shown by the dashed lines in Fig. 2. The position of the first peak is equal to z_v for the more spherical dodecahedra and icosahedra, and the sharp interlayer feature for tetrahedra also occurs at $z = z_v$.

The orientational ordering is investigated using the orientational order parameter profile $P_1(z) = [\langle \sum_{i=1}^N \cos\theta_i \delta(z - z_i) \rangle / \langle \sum_{i=1}^N \delta(z - z_i) \rangle - P'_{1,\text{iso}}] / [1 - P'_{1,\text{iso}}]$. Here, θ_i is the minimum of the angles between the normals of the faces and the normal to the wall pointing away from the system for particle i and $P'_{1,\text{iso}}$ is the average of $\frac{1}{N} \sum_{i=1}^N \cos\theta_i$ over all orientations. The definition of $P_1(z)$ is such that $P_1(z) = 1$ implies that one of the faces (which are all equivalent for regular polyhedra) is perfectly aligned with the wall and $P_1(z) = 0$ when all orientations of the polyhedron are equally probable. The orientational order parameter profile is shown in Fig. 3. Obviously, perfect face alignment is always found for z equal to z_f ,

denoted by the leftmost dashed line in Fig. 2 and the right border of the gray rectangles in Fig. 3. Tetrahedra show considerable misalignment compared to the average at somewhat larger height, which is somewhat underestimated by the theory. For the other shapes, the agreement between theory and simulations is nearly perfect, while the misalignment above the first layer is much less than for tetrahedra. Naturally, the nearly spherical icosahedra and dodecahedra show very little orientational order unless they are brought really close to the wall.

As mentioned above, DFT calculations are a natural method to obtain interfacial tension, in this case, of the wall-fluid interface γ_{wf} , as $\Omega = \Omega_b + 2\gamma_{\text{wf}}A$ in our fluid of hard polyhedra between two hard walls, where Ω_b is the grand-canonical free energy of the bulk reference fluid with volume LA . In Fig. 3(f), γ_{wf} is shown to increase as the number of faces of the polyhedron decreases, which is a natural result of the decrease in orientational freedom in the fluid near the wall [corresponding to a nonzero value of $P_1(z)$ in Figs. 3(a)–3(e)] with increasing anisotropy of the particles.

Finally, we apply the DFT to mixtures of polyhedra. We consider a 2:1 mixture of tetrahedra and octahedra [36] with the same edge length for both species. The constituents of this mixture, two tetrahedra and an octahedron, can form a parallelepiped that has a maximum packing fraction of 1. The corresponding crystal contains flat layers, so we might expect a similar structure at the wall; see the inset of

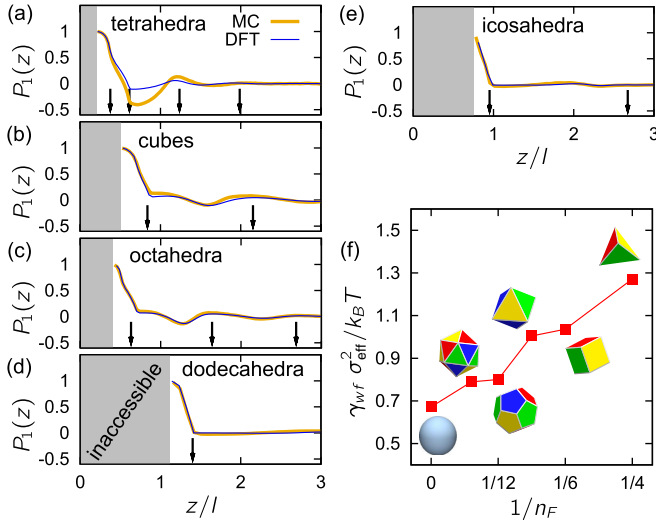


FIG. 3 (color online). (a)–(e) Orientational order parameter profiles $P_1(z)$, which measure the degree of face-wall alignment in one-component systems for the Platonic solids (see Fig. 1) as a function of the dimensionless distance to the wall z/l . DFT (dark or blue lines) is compared to MC simulation results (light or orange lines). The gray rectangles denote the z ranges that are inaccessible due to overlap with the wall for all orientations. The arrows denote the z positions of the peaks in the center-of-mass density profile (Fig. 2). (f) The dimensionless wall-fluid interfacial tensions $\gamma_{wf} \sigma_{eff}^2 / k_B T$ from DFT calculations for the Platonic polyhedra with n_F faces and spheres ($n_F = \infty$) [27], where σ_{eff} is the diameter of a sphere with the same volume as the particle of interest.

Fig. 4. To allow an easy comparison to the pure systems of octahedra and tetrahedra, we use the same packing fraction $\eta = 0.3$ as for the one-component systems. The resulting center-of-mass density profiles from the theory and the simulations are shown to agree very well in Fig. 4. Focusing on the first peak, we see that the octahedral peak has almost the same position in the mixture as in the one-component system [Fig. 2(c)]. In comparison, the changes in the tetrahedral peak are remarkable: The sharp feature at $z = z_v$ is much less pronounced, the peak near the wall is broader, and its maximum has shifted toward higher z values. This is the exact opposite of what one would expect from the crystalline layer [see Fig. 4 (inset)], where the peak at $z = z_v$ would actually be enhanced. Clearly, the behavior of the polyhedra near the wall is not so easy to predict from simple considerations, while our DFT is able to predict the complex structure accurately.

In conclusion, we propose a fundamental-measure density functional theory for polyhedral particles, which shows excellent overall agreement with simulation results. In future work, the theory could be applied to crystals of convex polyhedra. Nonconvex polyhedra have recently been synthesized in the form of nanoparticles, and their packing has been studied using a packing algorithm [11]. The theory presented here can in principle be extended to nonconvex particles at the cost of an additional

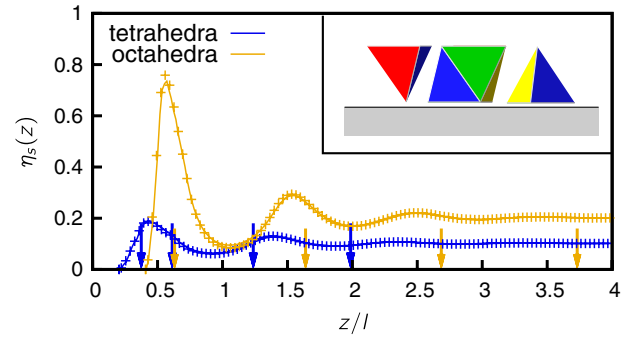


FIG. 4 (color online). Partial center-of-mass density profiles $\eta_s(z)$ for a 2:1 mixture of tetrahedra (dark or blue lines) for $s = 1$ and octahedra (light or orange lines) for $s = 2$ with equal edge lengths l as a function of the dimensionless distance to the wall z/l . The symbols, lines, and arrows of the same color denote the simulation results for the mixture, the theory for the mixture, and the z positions of the bulk $\eta(z)$ peaks, respectively, of the corresponding species. The results should be compared to those in the bulk; see Fig. 2(a) for tetrahedra and Fig. 2(c) for octahedra. The inset shows an example configuration as expected from expanding a close-packed layer.

approximation [35]. The theory can also be directly applied to the polyhedral approximation of a colloid or nanoparticle that results from modeling [37,38] of the synthesis process or a direct measurement [39]. Polyhedral molecules [19,40] and nanoparticles [2] or colloids with significant (depletion) attractions could be modeled by adding the attractions as a perturbation on top of DFT for hard polyhedra. Finally, nonequilibrium systems of hard polyhedra could be investigated using the dynamic version of DFT [33,41–43], which presupposes the existence of a free energy functional for the corresponding equilibrium system.

We thank Matthias Schmidt for useful discussions. The SFB TR6 (Project No. D3) is acknowledged for financial support.

-
- [1] R. Zheng, H. Gu, B. Xu, K. Fung, X. Zhang, and S. Ringer, *Adv. Mater.* **18**, 2418 (2006).
 - [2] J. Henzie, M. Grünwald, A. Widmer-Cooper, P.L. Geissler, and P. Yang, *Nat. Mater.* **11**, 131 (2011).
 - [3] L. Rossi, S. Sacanna, W.T.M. Irvine, P.M. Chaikin, D.J. Pine, and A.P. Philipse, *Soft Matter* **7**, 4139 (2011).
 - [4] M.H. Huang and P.-H. Lin, *Adv. Funct. Mater.* **22**, 14 (2012).
 - [5] Z. Quan and J. Fang, *Nano Today* **5**, 390 (2010).
 - [6] L.A. Woldering, L. Abelmann, and M.C. Elwenspoek, *J. Appl. Phys.* **110**, 043107 (2011).
 - [7] D.H. Gracias, J. Tien, T.L. Breen, C. Hsu, and G.M. Whitesides, *Science* **289**, 1170 (2000).
 - [8] M. Senechal, *Mathematics magazine* **54**, 227 (1981).
 - [9] S. Torquato and Y. Jiao, *Nat. Mater.* **460**, 876 (2009).
 - [10] U. Betke and M. Henk, *Comput. Geom.* **16**, 157 (2000).

- [11] J. de Graaf, R. van Roij, and M. Dijkstra, *Phys. Rev. Lett.* **107**, 155501 (2011).
- [12] A. Haji-Akbari, M. Engel, A. S. Keys, X. Zheng, R. G. Petschek, P. Palfy-Muhoray, and S. C. Glotzer, *Nat. Mater.* **462**, 773 (2009).
- [13] A. Haji-Akbari, M. Engel, and S. C. Glotzer, *Phys. Rev. Lett.* **107**, 215702 (2011).
- [14] U. Agarwal and F. A. Escobedo, *Nat. Mater.* **10**, 230 (2011).
- [15] P. F. Damasceno, M. Engel, and S. C. Glotzer, *Science* **337**, 453 (2012).
- [16] A. Haji-Akbari, M. Engel, and S. C. Glotzer, *J. Chem. Phys.* **135**, 194101 (2011).
- [17] R. Gibbons, *Mol. Phys.* **17**, 81 (1969).
- [18] J. Kolafa and I. Nezbeda, *Mol. Phys.* **84**, 421 (1995).
- [19] P. R. Bienkowski and K.-C. Chao, *J. Chem. Phys.* **63**, 4217 (1975).
- [20] R. Evans, *Adv. Phys.* **28**, 143 (1979).
- [21] Y. Singh, *Phys. Rep.* **207**, 351 (1991).
- [22] J. Wu and Z. Li, *Annu. Rev. Phys. Chem.* **58**, 85 (2007).
- [23] Y. Rosenfeld, *Phys. Rev. E* **50**, R3318 (1994).
- [24] Y. Rosenfeld, *Phys. Rev. Lett.* **63**, 980 (1989).
- [25] H. Hansen-Goos and K. Mecke, *Phys. Rev. Lett.* **102**, 018302 (2009).
- [26] H. Hansen-Goos and K. Mecke, *J. Phys. Condens. Matter* **22**, 364107 (2010).
- [27] R. Roth, *J. Phys. Condens. Matter* **22**, 063102 (2010).
- [28] M. Oettel, S. Görig, A. Härtel, H. Löwen, M. Radu, and T. Schilling, *Phys. Rev. E* **82**, 051404 (2010).
- [29] A. Härtel, M. Oettel, R. E. Rozas, S. U. Egelhaaf, J. Horbach, and H. Löwen, *Phys. Rev. Lett.* **108**, 226101 (2012).
- [30] A. Fortini, M. Dijkstra, M. Schmidt, and P. P. F. Wessels, *Phys. Rev. E* **71**, 051403 (2005).
- [31] B. B. Laird and R. L. Davidchack, *J. Chem. Phys.* **132**, 204101 (2010).
- [32] R. P. A. Dullens, M. C. D. Mourad, D. G. A. L. Aarts, J. P. Hoogenboom, and W. K. Kegel, *Phys. Rev. Lett.* **96**, 028304 (2006).
- [33] C. P. Royall, J. Dzubiella, M. Schmidt, and A. van Blaaderen, *Phys. Rev. Lett.* **98**, 188304 (2007).
- [34] P. Tarazona, *Phys. Rev. Lett.* **84**, 694 (2000).
- [35] See Supplemental Material at <http://link.aps.org/supplemental/10.1103/PhysRevLett.110.137801> for the calculation of the weight functions and technical details.
- [36] The volume of an octahedron is 4 times the volume of a tetrahedron, so the volume ratio [which is equal to the ratio between the $\eta_s(z)$ far away from the wall] between tetrahedra and octahedra is 1:2, i.e., the inverse of the number ratio.
- [37] N. Sasaki, Y. Murakami, D. Shindo, and T. Sugimoto, *J. Colloid Interface Sci.* **213**, 121 (1999).
- [38] C. Quilliet, C. Zoldesi, C. Riera, A. van Blaaderen, and A. Imhof, *Eur. Phys. J. E* **27**, 13 (2008).
- [39] P. A. Midgley and R. E. Dunin-Borkowski, *Nat. Mater.* **8**, 271 (2009).
- [40] S. R. Seidel and P. J. Stang, *Acc. Chem. Res.* **35**, 972 (2002).
- [41] U. M. B. Marconi and P. Tarazona, *J. Chem. Phys.* **110**, 8032 (1999).
- [42] A. J. Archer and R. Evans, *J. Chem. Phys.* **121**, 4246 (2004).
- [43] R. Wittkowski and H. Löwen, *Mol. Phys.* **109**, 2935 (2011).